

A reference sample of face-on bulgeless galaxies

I. D. Karachentsev^{1*}, V. E. Karachentseva²

¹*Special Astrophysical Observatory, Russian Academy of Sciences, N.Arkhыз, 369167 Russia*

²*Main Astronomical Observatory of National Academy of Sciences of Ukraine, Kiev 03143 Ukraine*

Accepted XXX. Received XXX; in original form XXX

ABSTRACT

We present a list of 220 face-on, almost bulgeless galaxies assumed to be counterparts to the objects from the Reference Flat Galaxy Catalog (RFGC). We selected the Sc, Scd and Sd-type galaxies according to their apparent axial ratio $\log(r_{25}) < 0.05$ and major standard angular diameter $\log(d_{25}) > 0.90$ as defined in HyperLEDA. The sample objects are restricted by the radial velocity $V_{LG} < 10000$ km/s and a declination of above -30 deg. The morphological composition of our sample is quite similar to that of RFGC. We notice the following common properties of face-on bulgeless galaxies. About half of them have bar-like structures occurring in the whole range of the absolute magnitudes of galaxies: from -17 to -22 mag. An essential part of our sample (27–50%) exhibit distorted spiral patterns. The galaxies do not show significant asymmetry in numbers of the “S”- and “Z”-like spin orientation. The mean (pseudo)bulge-to-total mass ratio for the sample is estimated as 0.11. Due to a negligible internal extinction, low-light background, and small projection effect, the face-on Sc–Sd discs are suitable objects to recognize their central nuclei as moderate-mass BH candidates. About 40–60% of the galaxies have distinct unresolved nuclei, and their presence steeply depend on the luminosity of the host galaxy.

Key words: galaxies: bulges – galaxies: spiral – galaxies: nuclei

1 INTRODUCTION

The Hubble’s morphological classification of galaxies and the improved classification by de Vaucouleurs et al. (1976) are based on the ratio of luminosities of spheroidal and disc components of a galaxy (the bulge-to-disc ratio). This ratio can be easily estimated visually in the case of “edge-on” galaxies. Karachentsev et al. (1993, 1999) compiled catalogues classifying such galaxies. The RFGC catalogue contains 4236 galaxies with angular diameters of more than $0.6'$ and the apparent axial ratios $a/b > 7$ distributed over the whole sky except for the Milky Way region. Later, Karachentseva et al. (2016) compiled a sample of 817 extremely thin spiral galaxies with the axial ratios $(a/b)_B > 10.0$ and $(a/b)_R > 8.5$ in the blue and red bands of the Palomar Sky Survey, respectively. Over 80% of such ultra-flat (UF) galaxies refer to the following morphological types: Sc (T=5), Scd (T=6), and Sd (T=7). These objects are interesting for almost full absence of a spheroidal stellar subsystem in them. Occurrence of a large number of such bulgeless galaxies impose challenge to hierarchic clustering models of galaxy formation (Kormendy et al. 2010). The UF galaxies are isolated objects located in the low-density regions which makes it difficult to estimate their total mass from orbital motions of rare satellites (Karachentsev et al. 2016). Studies of star-formation rates of UF galaxies are complicated by the presence of a considerable internal light extinction, especially in the far ultraviolet (Melnyk et al. 2017).

The projection effect and internal extinction conceal important structural elements of thin edge-on galaxies: central unresolved nuclei, bars, and specific features of the spiral pattern. In order to estimate the statistical abundance of those structural elements of UF galaxies, a quite representative sample of face-on bulgeless galaxies is required. The present paper considers such a sample. The appearance of the following high angular resolution sky surveys in various optical bands facilitated its creation: SDSS (Abazajian et al. 2009) and Pan-STARRS1 (Chambers et al. 2016). Going forward, we intend to use the

* E-mail: ikar@sao.ru

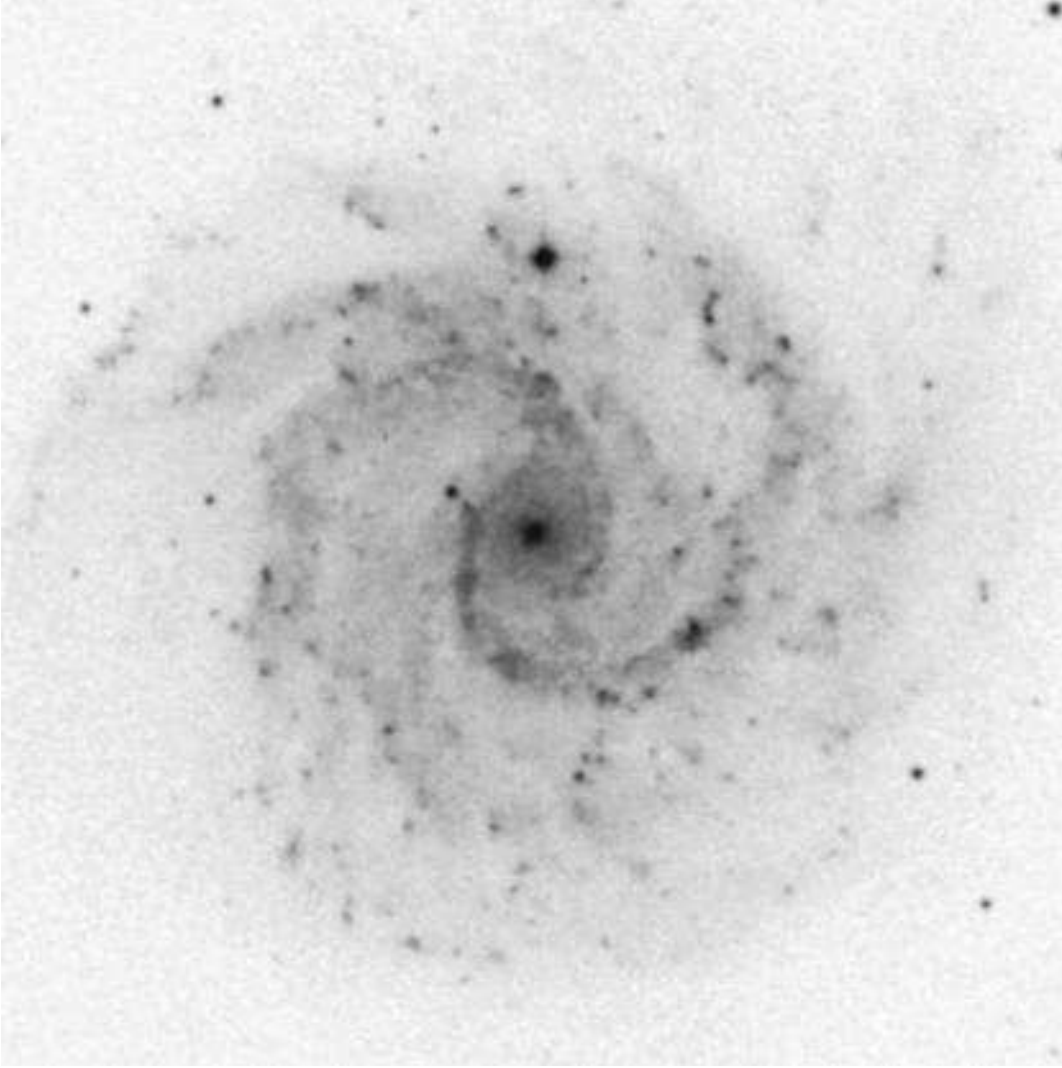


Figure 1. Face-on Scd galaxy NGC 3184. Reproduction from POSS-II of the $7' \times 7'$ size, North – at the top, East – on the left.

sample of face-on bulgeless galaxies to derive a more accurate estimate of the internal extinction in galactic discs, to estimate the characteristic star-formation rate in them, as well as to establish a membership of bulgeless galaxies in various elements of the cosmic large-scale structure.

2 SAMPLE SELECTION

To compile an analogue of the sample of UF galaxies, not edge-on, but face-on, we have undertaken the following procedures. We selected the galaxies in the HyperLEDA database (Makarov et al. 2014), which meet the conditions:

$$\log(r_{25}) \leq 0.05, \quad (1)$$

where $r_{25} = a/b$ is the apparent axial ratio (major/minor axis) measured at a standard isophote level of $25^m/\square''$ in the B band;

$$\log(d_{25}) \geq 0.90, \quad (2)$$

d_{25} is the standard angular diameter (major axis) in units $0.1'$ and determined from the same isophote;

$$4.0 < T < 8.5, \quad (3)$$

i.e., the morphological type according to the de Vaucouleurs's scale covers the range from Sbc to Sdm/Sm;

$$V_{LG} < 10000 \text{ km/s}, \quad (4)$$

V_{LG} is the radial velocity of a galaxy relative to the Local Group centroid.

Our result was the sample of 537 objects. Further, we examined visually all the selected galaxies and left only the cases with the refined morphological types

$$5 \leq T \leq 7. \quad (5)$$

As follows from the data (Heidmann et al. 1972, Karachentsev et al. 2017), the Sc, Scd, and Sd galaxies have the highest true axial ratio a/b and, consequently, the minimum bulges.

For reasons of homogeneity, in the final sample we left only the objects with the declination

$$DEC > -30^\circ, \quad (6)$$

which are given in the Pan-STARRS1 survey that we used to classify the structural features of spiral galaxies. It resulted in decreasing our sample to 220 galaxies. Table 1 presents the list of these Sc–Scd–Sd galaxies viewed at a slight angle. The list includes seven bright nearby galaxies: IC 342 (3.28 Mpc), NGC 5068 (5.15 Mpc), M 101 (6.95 Mpc), NGC 6946 (7.73 Mpc), NGC 3344 (9.82 Mpc), NGC 628 (10.19 Mpc), and NGC 3184 (11.12 Mpc), the distances to which are measured with an accuracy of $\sim 5\%$ from the tip of the red giant branch, cepheids or supernovae. Figure 1 which is the reproduction from the Palomar Sky Survey (POSS-II) shows the image of the last one.

Table 1 presents the observed main characteristics of 220 face-on galaxies described in the Table Notes.

Table 1: Basic properties of the face-on bulgeless galaxies.

Name	B_t	V_{LG}	V_{max}	modD	T	Bar	Spin	Asm	Nuc	M_B
	mag	km/s	km/s	mag						mag
(1)	(2)	(3)	(4)	(5)	(6)	(7)	(8)	(9)	(10)	(11)
NGC7816	13.91	5443	75	34.42	c	0	S	0	2,2	-20.87
UGC00044	16.70	6475	40	34.81	d	2	S	0	0,0	-18.33
UGC00048	15.60	4596	34	34.07	cd	2	Z	2	0,0	-19.15
NGC7834	15.35	5434	52	34.40	cd	1	S	1	1,0	-19.76
NGC0039	14.34	5121	80	34.30	c	0	Z	0	2,2	-20.38
UGC00160	16.50	4939	55	34.23	cd	0	S	0	1,0	-17.97
PGC1075005	15.57	3378		33.33	cd	0	Z	1	1,0	-18.00
PGC002257	15.41	4290		33.94	c	2	Z	1	0,0	-18.64
IC1562	13.60	3771	22	33.56	c	0	Z	1	2,2	-20.10
NGC0198	13.10	5414	97	34.40	c	0	S	0	2,2	-21.48
IC0043	13.95	5103	78	34.28	c	2	Z	1	2,2	-20.69
NGC0236	14.43	5804	52	34.55	c	2	S	2	2,2	-20.32
NGC0255	12.41	1694	68	31.70	c	2	Z	2	1,1	-19.49
IC0056	15.15	6174	60	34.69	cd	0	S	2	2,1	-19.75
UGC00626	14.97	5874		34.58	c	0	Z	0	2,1	-19.90
ESO412-013	15.00	5677		34.51	c	0	S	1	1,1	-19.67
ESO542-004	15.00	5657		34.50	d	2	S	2	1,0	-19.60
IC1666	14.35	5108	70	34.30	cd	1	S	0	2,2	-20.27
PGC005023	15.78	2372	18	32.51	cd	2	S	0	0,0	-16.87
UGC00929	14.82	7581	31	35.15	cd	0	Z	1	2,2	-20.60
NGC0575	13.72	3337	62	33.33	c	2	S	0	2,2	-19.94
UGC01087	14.83	4654	59	34.19	c	0	S	1	2,1	-19.66
NGC0628	9.71	828	21	30.03	c	0	Z	0	2,2	-20.68
UGC01148	15.45	4951	66	34.30	c	0	Z	1	1,0	-19.59
ESO543-021	14.95	5754		34.54	c	1	Z	1	1,0	-19.72
UGC01347	13.50	5759	52	34.57	c	2	S	0	2,2	-21.44
PGC007210	14.97	8166	99	35.32	c	2	S	2	1,1	-20.54
UGC01478	14.56	5024	41	34.24	c	2	S	0	1,1	-20.25
UGC01546	14.76	2527	38	32.70	c	2	S	0	1,0	-18.35
PGC007942	15.00	5332	53	34.37	cd	0	S	0	1,1	-19.57
PGC008142	14.91	8061		35.30	c	0	Z	0	1,1	-20.61
UGC01626	14.42	5762	73	34.57	c	2	S	1	1,1	-20.54
UGC02043	14.96	5316		34.40	c	0	Z	0	2,2	-20.05
IC0239	11.89	1096	48	30.87	cd	2	S	0	1,0	-19.34
UGC02094	13.74	5314	116	34.39	c	0	S	1	2,2	-20.98
UGC02121	14.95	6580	36	34.85	c	0	S	0	2,2	-20.16
UGC02122	14.41	5243	59	34.35	c	0	S	1	2,2	-20.66
ESO479-022	15.39	7266		35.07	c	2	S	1	0,0	-19.89
UGC02174	15.09	5296	39	34.39	c	1	S	0	2,1	-19.92
ESO546-011	14.52	4535	27	34.01	c	2	Z	1	1,0	-19.74
NGC1067	14.55	4700	59	34.11	c	2	Z	0	2,2	-20.43
UGC02323	15.66	8139	59	35.33	c	2	Z	0	2,2	-20.84
UGC02399	15.45	8065	86	35.31	c	2	S	1	2,2	-20.79

(1)	(2)	(3)	(4)	(5)	(6)	(7)	(8)	(9)	(10)	(11)
UGC02434	16.00	8108	87	35.32	cd	2	S	1	1,1	-20.21
PGC012008	15.00	9439		35.66	c	1	S	1	2,2	-20.95
UGC02623	15.59	4577	46	34.07	d	2	S	1	0,1	-19.57
UGC02671	17.00	7205	79	35.07	d	1	Z	1	1,1	-19.89
UGC02692	14.07	6337	82	34.77	c	0	Z	1	2,2	-21.10
UGC02712	15.50	7140	69	35.04	cd	2	S	1	2,1	-20.82
UGC02721	16.40	6506	25	34.84	d	2	Z	2	0,0	-19.12
NGC1325A	13.40	1262	18	31.11	d	0	S	1	2,0	-17.87
ESO548-035	13.49	4161	56	33.82	c	2	Z	1	2,2	-20.67
NGC1376	12.85	4137	70	33.82	c	0	S	2	2,2	-21.21
PGC013714	15.10	4308		33.91	cd	0	Z	1	2,1	-19.21
IC0342	9.68	239	72	27.68	c	0	S	1	2,2	-20.45
UGC02859	16.00	5645	88	34.54	c	2	Z	0	2,2	-20.51
UGC02932	15.11	4995	88	34.26	d	0	S	0	1,0	-19.92
IC0370	14.94	9649	57	35.72	c	2	Z	0	2,2	-21.33
UGC03051	16.00	6900	87	34.98	cd	0	Z	1	1,1	-20.00
NGC1599	14.10	3947	41	33.73	c	0	S	2	2,1	-19.86
PGC015609	15.37	9253		35.63	c	2	S	1	2,2	-20.63
IC2102	14.52	3543	34	33.51	cd	2	Z	2	0,0	-19.26
IC0391	12.98	1768	55	32.12	c	0	S	1	1,1	-19.73
ESO552-047	15.26	6568		34.87	c	2	Z	0	2,1	-20.12
UGC03308	16.50	8459	45	35.44	d	0	S	0	2,2	-20.36
PGC017323	13.49	2016	33	32.30	d	0	S	2	1,0	-19.20
PGC018031	14.84	6986	71	35.03	c	2	S	1	2,2	-21.34
UGC03364	16.00	4630	59	34.15	cd	0	S	0	2,1	-18.76
IC0441	14.40	2042	47	32.34	c	2	Z	0	1,0	-19.18
UGC03574	13.20	1551	62	31.34	cd	0	S	1	2,1	-18.41
UGC03602	14.76	1983	49	32.34	d	0	S	0	0,0	-18.17
UGC03703	15.35	7260	22	35.14	c	2	S	0	2,1	-20.16
UGC03701	14.80	3085	54	33.30	cd	2	Z	2	1,0	-18.78
UGC03806	15.26	5414	90	34.51	cd	2	Z	1	2,2	-19.73
UGC03825	15.06	8303	92	35.43	c	2	Z	1	2,2	-20.82
UGC03875	15.24	5303	85	34.46	cd	2	S	1	0,0	-19.59
UGC03886	16.00	5006	48	34.33	c	2	S	1	2,0	-18.66
UGC03924	15.66	5032	41	34.35	d	0	S	1	0,0	-18.79
UGC04074	13.75	7263		35.14	c	0	S	1	2,2	-21.60
NGC2500	12.22	558	41	30.47	d	1	S	1	2,1	-18.47
NGC2514	14.01	4728	50	34.23	c	2	Z	2	2,1	-20.43
UGC04107	13.94	3557	63	33.61	c	0	Z	1	2,2	-19.92
PGC086610	16.40	4718	21	34.23	d	0	Z	1	0,0	-18.05
PGC023378	14.49	4359	50	34.05	cd	0	Z	1	2,1	-19.83
UGC04380	15.05	7554	52	35.24	c	0	Z	0	2,1	-20.53
UGC04445	15.06	6435	18	34.88	c	0	S	0	2,1	-20.19
IC0509	13.83	5398	36	34.52	c	2	Z	1	2,1	-20.97
NGC2607	14.95	3447	25	33.56	c	0	S	2	2,2	-18.86
UGC04536	15.42	7507		35.22	c	2	S	1	2,2	-20.31
NGC2661	13.86	3958	41	33.87	cd	0	Z	2	2,2	-20.23
UGC04669	15.46	3988	68	33.89	d	2	Z	1	0,0	-18.63
UGC04853	15.24	2512	28	32.94	cd	2	S	2	0,0	-17.99
PGC026687	14.72	3380		33.54	cd	0	Z	1	1,0	-19.04
UGC05015	15.30	1598	51	32.02	cd	0	S	1	1,0	-16.85
UGC05153	15.65	8044		35.38	c	0	S	0	2,1	-19.95
UGC05169	15.44	7699		35.29	d	2	Z	0	2,0	-19.99
NGC2967	12.28	1679	57	32.16	c	0	S	1	2,2	-20.37
UGC05274	14.92	5764	59	34.68	cd	0	Z	2	2,1	-19.99
ESO566-019	13.99	3429	71	33.56	cd	2	Z	2	1,0	-19.83
ESO499-011	15.01	2342	32	32.77	d	2	S	2	0,0	-18.07
PGC028556	14.84	7163	26	35.14	c	0	Z	1	2,1	-20.62
ESO567-010	14.44	2779	19	33.13	cd	2	Z	1	1,0	-19.05
PGC029301	15.24	9103		35.66	c	2	Z	0	2,2	-20.71
UGC05474	14.89	5847	64	34.71	cd	2	S	1	0,1	-19.98
UGC05483	15.13	6014	36	34.77	c	0	Z	0	2,0	-19.93
PGC029882	14.54	9046		35.64	c	2	S	0	2,2	-21.45
PGC029929	14.30	3214	38	33.44	d	2	S	1	2,0	-19.56
NGC3184	10.41	588	51	30.33	cd	0	Z	1	2,2	-20.01
PGC030452	14.78	6363		34.90	c	0	S	1	1,1	-20.27
PGC030830	14.91	7209		35.14	c	0	Z	1	2,1	-20.40

(1)	(2)	(3)	(4)	(5)	(6)	(7)	(8)	(9)	(10)	(11)
NGC3344	10.50	499	69	29.96	c	2	Z	0	2,2	-19.64
PGC031979	14.05	1838	68	32.34	d	0	S	2	0,0	-18.50
PGC032091	14.45	2268	59	32.77	cd	2	S	2	1,0	-18.56
NGC3433	13.30	2553	116	33.01	c	0	S	1	2,2	-19.89
PGC032817	15.28	8017		35.39	cd	2	S	2	2,1	-20.37
NGC3506	13.16	6252	85	34.87	c	0	Z	2	2,2	-21.92
UGC06130	15.02	8151	98	35.42	c	2	S	1	2,0	-20.62
UGC06194	14.62	2551	48	33.01	cd	2	S	2	0,0	-18.49
PGC034006	14.13	7543	73	35.26	c	2	S	1	2,2	-21.49
NGC3596	11.79	1062	50	31.32	cd	0	S	1	2,2	-19.68
UGC06326	15.76	2094	53	32.62	d	2	Z	1	0,0	-17.00
UGC06335	14.91	3026	23	33.30	cd	0	S	1	1,0	-18.49
UGC06429	13.78	3849	23	33.80	c	0	Z	0	2,1	-20.14
IC0696	14.50	6132	74	34.83	cd	2	S	1	1,1	-20.60
UGC06528	14.12	3365	15	33.54	c	2	S	1	1,0	-19.55
NGC3763	12.90	5651	100	34.65	c	2	S	1	2,2	-21.99
PGC036269	15.59	6462	86	34.92	c	0	S	1	1,0	-19.53
PGC036353	14.14	2868		33.25	c	0	S	1	1,0	-19.52
NGC3938	10.87	841	38	30.87	c	0	Z	1	2,2	-20.12
ESO573-002	15.50	5550	57	34.06	c	0	S	1	2,1	-19.49
NGC4136	11.90	560	38	31.09	c	1	Z	2	2,2	-19.32
NGC4195	15.29	4473	33	34.13	cd	2	S	2	0,0	-19.06
NGC4303	10.16	1422	66	31.36	c	2	Z	1	2,2	-21.34
NGC4303A	13.53	1135	50	31.45	cd	0	S	1	0,0	-18.07
IC3267	14.12	1103	24	32.86	c	0	S	1	2,1	-18.87
IC3271	14.57	7083	69	35.13	c	2	S	2	1,1	-20.79
NGC 4411B	12.98	1149	35	32.14	cd	0	Z	1	2,0	-19.38
NGC4535	10.56	1841	122	31.05	c	2	S	1	2,2	-20.65
NGC4571	11.92	244	67	30.93	cd	0	Z	2	2,2	-19.27
NGC4653	12.77	2471	92	33.08	c	0	Z	1	2,2	-20.50
PGC042868	13.03	1259	49	31.64	d	0	S	2	2,0	-18.81
ESO574-029	13.67	6081		34.80	c	1	S	0	2,2	-21.45
NGC4688	12.92	857	20	31.03	d	2	Z	2	1,0	-18.32
NGC4900	11.89	836	36	31.86	c	2	S	1	1,2	-20.11
UGC08153	14.49	2742	54	33.16	cd	2	Z	2	0,0	-18.81
PGC045690	15.86	4892		34.33	c	0	Z	0	1,0	-18.59
NGC5068	10.64	471	38	28.56	cd	2	S	2	0,1	-18.45
UGC08436	15.03	3019	28	33.30	d	0	Z	0	0,0	-18.43
NGC5154	14.73	5586	64	34.62	c	0	S	1	2,2	-20.03
PGC048087	14.45	2315	40	32.81	d	2	Z	1	1,0	-18.75
NGC5260	13.58	6313	119	34.87	c	2	Z	0	2,2	-21.69
ESO445-76	14.73	2511	44	32.94	d	0	S	1	0,0	-18.57
UGC08877	15.18	2464	17	32.91	d	2	S	0	0,0	-17.84
NGC5405	14.52	6846	43	35.06	c	0	Z	1	2,2	-20.78
PGC049982	16.00	9208		35.67	c	0	S	0	2,0	-19.52
NGC5457	8.36	374	75	29.26	c	1	S	2	2,2	-20.97
NGC5434	13.94	4587	18	34.21	c	0	Z	0	2,1	-20.46
UGC09008	15.29	5305	55	34.52	cd	0	S	0	1,0	-19.35
NGC5468	12.95	2734	54	33.40	c	1	Z	2	2,2	-20.63
NGC5476	13.34	2530	80	32.97	cd	0	Z	1	1,2	-19.81
NGC5494	13.30	2428	104	32.99	c	0	S	1	2,2	-20.08
ESO446-031	13.60	2471	51	32.91	cd	2	Z	1	1,0	-19.69
UGC09144	15.95	7883		35.35	cd	0	S	1	2,0	-19.50
UGC09216	14.51	5618	106	34.63	c	0	S	0	2,0	-20.25
NGC5660	12.38	2458	55	32.91	c	0	Z	1	2,2	-20.70
UGC09317	15.00	4476	21	34.15	cd	2	S	1	0,0	-19.33
ESO580-014	14.55	5955	37	34.74	cd	2	S	1	1,2	-20.67
UGC09837	13.81	2849	71	33.19	c	2	S	2	1,1	-19.52
UGC09945	14.19	6857	97	35.04	c	0	Z	1	2,2	-21.16
IC1132	14.37	4604	45	34.19	c	2	Z	1	2,1	-20.17
UGC09982	15.26	7896	45	35.33	cd	2	Z	0	1,0	-20.21
NGC5989	13.56	3079	68	33.33	cd	0	S	1	2,1	-19.92
UGC10020	14.44	2175	25	32.66	d	0	S	1	1,0	-18.51
PGC056010	15.42	4619	30	34.21	cd	2	S	0	0,0	-19.01
PGC056318	15.33	5998		34.75	c	2	S	0	2,0	-19.60
PGC056639	15.77	8371		35.47	cd	2	S	0	2,2	-20.78
NGC6143	13.92	5521	124	34.57	c	2	S	1	2,2	-20.80

(1)	(2)	(3)	(4)	(5)	(6)	(7)	(8)	(9)	(10)	(11)
PGC058201	15.69	8562	54	35.51	c	2	Z	1	1,2	-20.12
UGC10427	15.19	9036	57	35.63	c	2	S	2	2,2	-20.61
IC1221	14.59	5706	18	34.63	cd	0	S	1	2,2	-20.21
UGC10590	14.06	3287		33.46	cd	2	Z	0	1,1	-19.60
IC1236	14.23	6171	45	34.80	c	2	Z	0	2,2	-21.01
AGC260883	16.07	9059	29	35.63	cd	0	S	1	0,0	-19.73
UGC10956	15.64	6825		35.00	c	2	S	0	2,2	-20.61
NGC6493	15.44	6199		34.80	cd	2	S	2	2,1	-19.58
UGC11064	14.40	7257	101	35.05	c	2	Z	0	2,2	-20.92
UGC11214	15.00	2834	36	33.10	cd	2	Z	2	0,0	-19.15
UGC11302	16.00	4324	55	33.99	d	2	S	1	0,0	-18.77
NGC6711	13.71	4944	84	34.30	c	2	Z	1	2,2	-21.02
UGC11430	14.41	5769	47	34.62	c	0	Z	2	2,2	-20.68
NGC6821	13.62	1680	54	31.86	d	2	Z	2	0,0	-19.70
NGC6946	9.75	349	98	29.44	c	0	Z	2	2,2	-21.20
PGC902799	16.30	3584	42	33.51	c	0	S	1	0,0	-17.50
UGC11636	16.00	2859	62	33.10	cd	2	S	1	0,0	-19.14
PGC065744	14.62	5810		34.58	c	0	Z	0	2,2	-20.38
PGC3083038	14.44	8486		35.43	c	2	Z	1	2,2	-21.39
NGC7137	13.05	1977	46	32.16	c	2	Z	0	2,2	-19.79
UGC11816	14.83	4962	52	34.26	c	2	Z	1	1,1	-20.10
UGC11834	14.45	3554	79	33.49	c	2	Z	0	1,0	-19.41
ESO532-008	15.29	6365		34.78	c	2	Z	1	0,0	-19.75
IC1418	15.23	8552	93	35.44	c	0	Z	2	2,2	-20.47
PGC068549	14.23	5163		34.30	c	2	S	2	1,2	-20.58
ESO602-027	14.48	5835	21	34.57	c	2	S	2	0,1	-20.38
NGC7309	13.04	4168	49	33.82	c	2	S	2	2,2	-21.12
PGC133417	14.97	8965		35.54	c	2	S	1	2,1	-20.73
UGC12156	14.76	5483	53	34.47	c	2	S	1	2,1	-20.34
ESO603-011	15.01	8303		35.37	c	2	Z	1	2,1	-20.64
UGC12192	16.50	6789	25	34.94	d	2	Z	1	0,0	-19.05
IC5261	13.88	3347	65	33.30	cd	2	Z	2	2,1	-19.68
NGC7437	13.95	2364	44	32.55	cd	2	S	2	2,0	-18.81
NGC7495	13.76	5133	85	34.28	c	2	Z	1	2,2	-21.02
NGC7535	14.28	4884	50	34.17	cd	2	Z	2	2,1	-20.20
UGC12522	15.41	3033	47	33.10	d	2	S	1	0,0	-18.21
UGC12585	14.63	3899	40	33.66	d	2	S	1	1,0	-19.42
UGC12635	15.31	5400	36	34.40	cd	0	S	0	2,1	-19.38
PGC071751	14.74	8381	92	35.40	c	0	Z	2	2,2	-21.01
ESO605-016	13.23	7999	100	35.28	c	2	Z	1	2,2	-22.24
PGC072738	14.82	6024	59	34.65	c	2	S	2	2,2	-20.15
UGC12838	14.86	7375	56	35.09	c	0	S	1	2,2	-20.52
NGC7798	12.95	2650	34	32.81	c	0	S	1	2,2	-20.23

Notes: Columns contain the following data. (1) – the name of the galaxy in HyperLEDA. (2) – the apparent integrated B magnitude from HyperLEDA with some refinements from NED (<http://ned.ipac.caltech.edu>), and other sources. (3) – the radial velocity relative to the Local Group centroid. (4) – the rotation amplitude of a galaxy from HyperLEDA. (5) – the distance modulus from HyperLEDA; in some cases: NGC 2500, NGC 4136, NGC 4303, NGC 4535, NGC 4571, NGC 4653, NGC 4900, and NGC 6946, the distance moduli were updated with the latest observational data. (6) – the morphological type: Sc, Scd, or Sd. (7) – the presence (“2”) or absence (“0”) of a bar; uncertain cases of a diffuse or short bar are marked with “1”. (8) – the “S”- or “Z”-like spin orientation of spiral arms. (9) – the presence (“2”) or absence (“0”) of a significant asymmetry of the spiral structure; (10) – the presence (“2”) or apparent absence (“0”) of an unresolved nucleus in a galaxy, while “1” characterizes the central concentration of a diffuse shape. The first digit refers to visibility in the optical range in the Pan-STARRS1 images, the second digit characterizes the visibility of the nucleus in the K_s band according to 2MASS (Jarrett et al. 2000). Case “2,2” corresponds to the presence of a distinct unresolved nucleus (a black hole candidate) in all the Pan-STARRS1 and 2MASS photometric bands. (11) – the absolute B band magnitude of a galaxy corrected for the Galactic extinction according to Schlegel et al. (1998). Table 2 presents the distribution of the galaxies from our sample by various structural features. As one can see, this sample demonstrates a considerable variety of structural forms of galaxies. Figure 2 shows a mosaic of images of 24 face-on galaxies. The galaxies in the mosaic are selected by the radial velocities in the range of [4500–5500] km/s, in which the median velocity lies. Here we do not show the images having corrupted sky background in Pan-STARRS1. Galaxy images of the sizes of $75'' \times 75''$ correspond to the g - band of the Pan-STARRS1 survey. In some galaxies, the spiral structure extends beyond the chosen format.

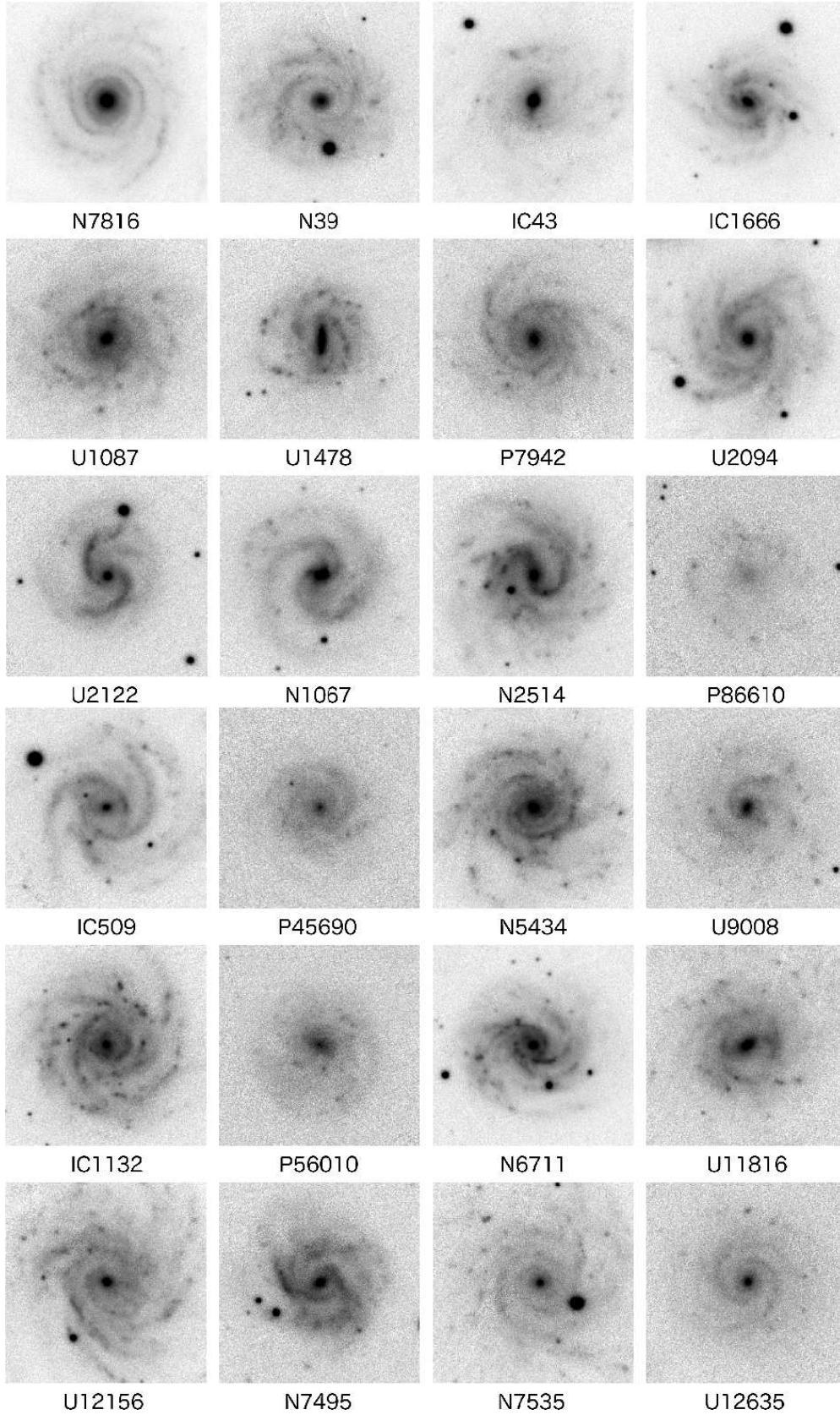


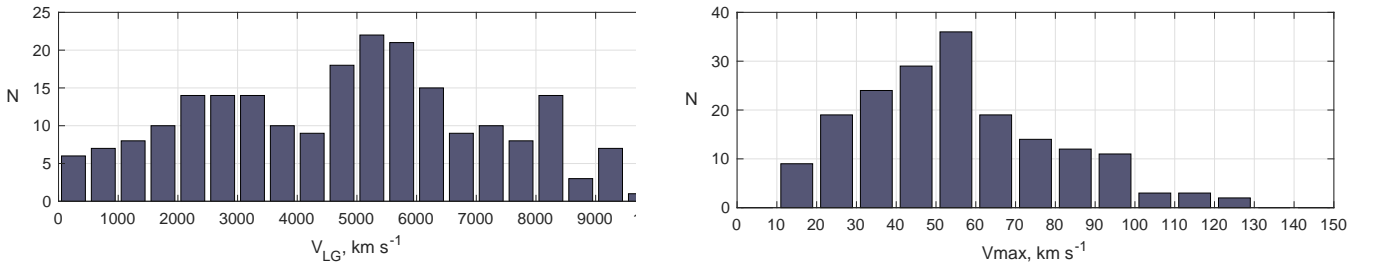
Figure 2. Mosaic images of 24 face-on galaxies of the Sc–Scd–Sd types with radial velocities in the range of 4500–5500 km/s. The reproductions are made from the images in the *g* band in the Pan-STARRS1 survey of the $75'' \times 75''$ size, North – at the top, East – on the left.

Table 2. Numbers of face-on Sc–Scd–Sd galaxies with different properties.

Property		N	(%)
Type	Sc	127	58
	Scd	62	28
	Sd	31	14
Bar	0	95	43
	1	11	5
	2	114	52
Spin	S	123	56
	Z	97	44
Asymmetry	0	60	27
	1	110	50
	2	50	23
B/Tot	0.05	15	7
	0.10	124	56
	0.15	64	29
	0.20	17	8
Nucl., Pan-STARRS1:	0	38	17
	1	53	24
	2	129	59
Nucl., 2MASS	0	78	35
	1	56	26
	2	86	39

Table 3. Numbers of face-on bulgeless galaxies with different nuclei visibility in the Pan-STARRS1 and 2MASS surveys.

Pan-STARRS1:	2	13	35	81
	1	31	17	5
	0	34	4	0
2MASS:	0	1	2	

**Figure 3.** Distribution of face-on bulgeless galaxies by radial velocities (the top panel) and by rotation amplitudes (the bottom panel).

3 BASIC PROPERTIES OF THE SAMPLE

The top panel of Fig.3 gives the distribution of the sample galaxies by radial velocities. The mean value for them, $\langle V_{LG} \rangle = +4845 \pm 170 \text{ km/s}$, within a standard error, coincides with the mean for the sample of 284 Sc, Scd, and Sd galaxies, $+5153 \pm 200 \text{ km/s}$, classified as ultra-flat (Karachentseva et al. 2016). It follows that both samples are taken from volumes having approximately the same depth. Here we should notice that the UF galaxies were selected by the angular diameter, $a > 1.2'$, which is 1.5 times greater than the assumed minimum diameter of face-on galaxies. This difference was justified by the fact that the 90° -turn of a face-on galaxy exactly one and a half times increases its apparent major diameter. Thus, selecting the major diameter $(d_{25})_{min} = 0.8'$ under condition (2) provided a sufficient depth and representativeness of the face-on bulgeless galaxies sample.

The bottom panel of Fig. 3 presents the distribution of our face-on galaxies by the observed rotation amplitude V_m . The pattern of this distribution with a mean of 56 km/s is determined not so much by masses of the galaxies but their small

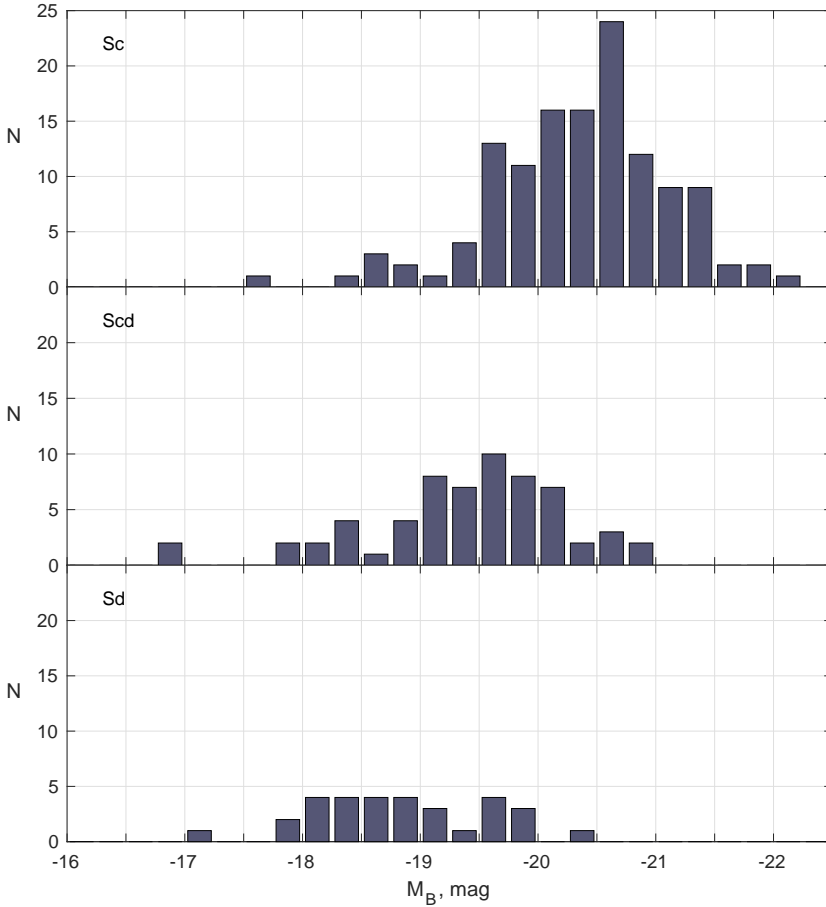


Figure 4. Distribution of face-on galaxies of the Sc, Scd, and Sd types by absolute magnitudes.

inclination angles. The mean full rotation amplitude of edge-on UF galaxies is $\langle V_m \rangle = 142$ km/s from the data of Table 1 (Karachentseva et al. 2016). Assuming it as a typical face-on galaxy, we obtain an estimate of the mean inclination angle in our sample $i = \arcsin(56/142) = 23^\circ$. With this characteristic inclination angle, the apparent axial ratio of the galaxy is $\log(r_{25}) \simeq 0.037$. Comparing it with condition (1), we can conclude that due to measurement errors of r_{25} a part of galaxies with the true inclination angle $i \simeq 0$ could fail to get into the sample under consideration. Also, omission of true face-on galaxies can result not only from errors in the axial ratio measurements but from the fact that many late-type galaxies are intrinsically lopsided. Then apparent axial ratios do not tell us inclinations in the normal way for circular discs.

As follows from the data given in Table 2, the majority of face-on galaxies (58%) were classified as the Sc-type spirals, while 28% of them are of the Scd type, and 14% – of the Sd type. This proportion is quite similar to the proportion of types of edge-on galaxies in the RFGC catalogue: 49% (Sc), 35% (Scd), and 16% (Sd), however, it differs markedly from the type proportion of UF galaxies: 25% (Sc), 28% (Scd), and 47% (Sd). Comparing our classification with that in HyperLEDA shows that the mean-square error in determining the morphological type of a galaxy is $\sigma(T) = 0.7$. Three panels of Fig. 4 show the distribution of face-on bulgeless galaxies of different types by the absolute magnitude M_B . The histograms show the well-known decrease of the mean luminosity (Kormendy, 1979; Karachentsev et al. 2017) along the Hubble sequence: $\langle M_B \rangle = -20.37 \pm 0.07$ for Sc, -19.40 ± 0.10 for Scd, and -18.82 ± 0.13 for Sd galaxies.

Favourable aspect angles and the absence of bright bulges make the face-on bulgeless galaxies suitable for statistical studies of the occurrence of bars in them. Except for a small number of cases (5%), the presence or absence of a bar in our sample galaxies is clearly distinguishable. Almost half of the face-on bulgeless galaxies (43%) demonstrate extended or short central bars. Figure 5 presents the distribution of galaxies with bars (the top panel) and without any (the bottom panel). As one can see, the bars are found both in high-luminosity galaxies and in dwarf discs. Both distributions are similar with a slight shift, $\Delta M_B = -0.15^m \pm 0.13^m$, towards the objects with bars. Most of the considered galaxies look like isolated objects. According to our preliminary estimations, they have no nearest significant neighbours within a radius of 100–200 kpc. Therefore, it can be affirmed that the presence of a bar in a thin disc is their intrinsic dynamic property almost independent of luminosity or linear sizes of the disc. Moreover, the fact that so many of these galaxies are isolated also suggests that their bars are not produced as a result of tidal force.

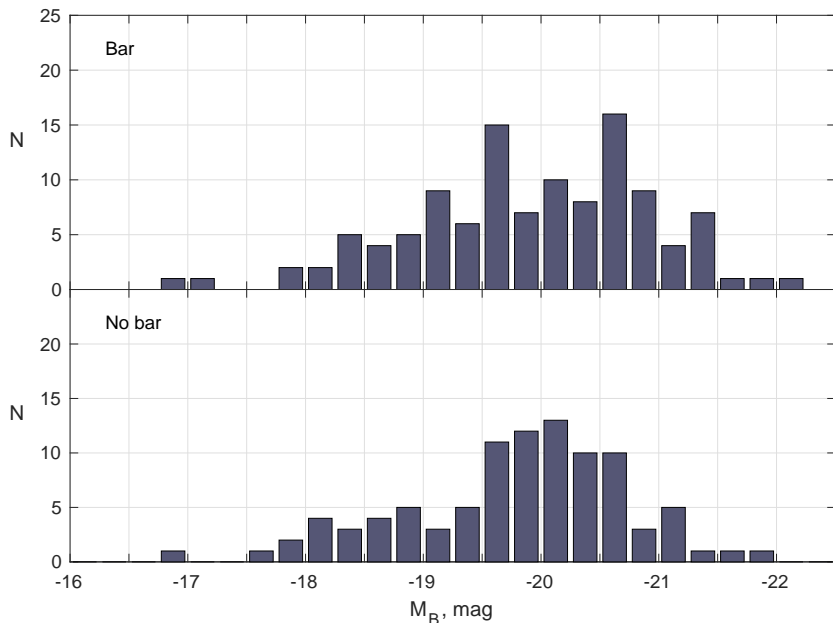


Figure 5. Distribution of face-on bulgeless galaxies with the signs of bar presence (the top panel) and without any (the bottom panel) by absolute magnitudes.

In modern models of the formation of galactic discs with their large angular momentum, the possibility of an ordered orientation of the galaxy spins with respect to the large-scale structure elements (filaments and walls) is allowed. Such a space organization of spins could manifest itself in the form of an excessive number of galaxies with “S”- or “Z”-like structures. The data in Table 2 show that the number of galaxies with different configuration of spiral arms, $N_S : N_Z = 123 : 97$, show only a statistically insignificant asymmetry on scales of ~ 5000 km/s. However, the absence of a preferred spin orientation should be controlled with a more representative sample of face-on galaxies. Parnovsky et al. (1994) noticed some evidence of anisotropy in the distribution of planes of edge-on galaxies in the FGC catalogue.

The spiral structure of our sample galaxies is characterized by varying degrees of asymmetry. About a quarter of galaxies (27%) are of a symmetric shape. Galaxies from another part of the sample (23%) show quite a strong asymmetry of spiral arms. The rest half of the sample galaxies have feebly-marked signs of asymmetry. The galaxies NGC 628 and NGC 3344 can be an example of a symmetrical spiral pattern. Considerable distortions of the spiral structure can be seen in the galaxy M 101 (NGC 5457); their apparent cause is the disturbance from the nearby companion NGC 5474, the structure of which is subject to even stronger tidal distortion. Statistics of absolute magnitudes show that the luminosity of strongly distorted galaxies, $\langle M_B \rangle = -19.75^m \pm 0.14^m$, is slightly lower than that of objects of a symmetrical structure, $\langle M_B \rangle = -20.05^m \pm 0.15^m$.

4 BULGE-TO-DISC RATIO

Based on the results of the surface photometry of 98 galaxies, Simien & de Vaucouleurs (1986) performed the decomposition of galaxies into the components: a bulge and a disc. According to their data, the luminosity ratio of bulge-to-disc in the blue band can be expressed as

$$B/D = 0.754 \times 10^{-T/5}.$$

For late-type galaxies, this yields the ratio of the bulge luminosity to the total luminosity: 0.070 for Sc, 0.045 for Scd, and 0.029 for Sd discs. Subsequently, Oohama et al. (2009) decomposed 737 galaxies of the morphological types $T = 1 \div 4$ using the SDSS photometric data in various bands. Extrapolation of their estimates of the B/D ratio towards later types with $T > 4$ results in a bulge proportion in the total luminosity of less than 10%. The similar work by Kim et al. (2016) on decomposition of 14233 SDSS galaxies in the r band gave the average relative luminosity of bulges of Sc galaxies less than 20%.

However, as it was shown by Kormendy (1982, 1993, 2013) and Kormendy & Kennicutt (2004), internal secular evolution of galaxy discs leads to formation of the central mass concentrations of stars and gas in the discs, generally called “pseudobulges” (PB). They look like classical, merger-built bulges but that were made slowly out of disc gas. The pseudobulges can be distinguished from classical bulges by their flatter shapes, nearly exponential brightness profiles as well as starburst activity.

It should be acknowledged that past papers such as Simien & de Vaucouleurs (1986) confused pseudobulges with classical bulges and actually estimated PB/D ratio.

Kormendy et al. (2010) used HST archive images to measure the brightness profiles of pseudobulges in M101 and NGC 6946. They showed that the above galaxies contain only tiny pseudobulges that make up less than 3 percent of the galaxy stellar mass. We kept this data as reference when visually assessing the proportion of a pseudobulge in the total luminosity of the galaxy. Taking into account the colour differences of a galaxy in the bands: g, r, i, z, y in the Pan-STARRS1 survey, we estimated the relative luminosity of a PB on scales: 5%, 10%, 15%, and 20%. Table 2 shows the result. For 85% face-on galaxies from our sample, the estimates of the relative luminosity of pseudobulge are 5–15% with the mean $\langle PB/Tot \rangle = 11\%$. This value almost coincides with the quantity $\langle (PB)/Tot \rangle = (13 \pm 3)\%$ obtained by Davis et al. (2018) for Sc–Sd galaxies.

There are more data on the decomposition of galaxies into a bulge and a disc in the literature. Some of them (Simard et al. 2011, Lackner & Gunn 2012, and Lange et al. 2016) number hundreds of thousands of objects. However, we could not use these data, because decomposition algorithms split most of our galaxies into separate nodes (then this is a sign that they have pseudobulges since star formation is often clumpy).

In general, it can be stated that the term “bulgeless” is fully justified in relation to spiral galaxies of the Sc–Sd types.

5 NUCLEI AS BLACK HOLE CANDIDATES

Galaxies without any evidence of a bright bulge and face-on oriented are the most suitable objects for searching for unresolved nuclei in their central parts as candidates to black holes (BH). We noticed the presence of an unresolved nucleus in a galaxy using a simple scheme: “2” is a distinct star-shaped core, “1” is the central concentration of a not completely unresolved, but rather diffuse shape, “0” is the absence of any visible signs of a nucleus. We applied this classification both to the images of galaxies in five optical bands of Pan-STARRS1 and to the view of the central region of the galaxy in the 2MASS K_s -band. Statistics of the visibility of nuclei in 220 galaxies of our sample is represented by the matrix in Table 3. The matrix of galaxy numbers has an asymmetric non-diagonal view with a shift towards a larger number of unresolved nuclei marked in the optical bands. This asymmetry is due to short galaxy exposures in the 2MASS survey.

From this matrix, we have selected two extreme cases: “2,2” or “0,0” that mean presence or absence of unresolved nuclei signs according to the data from both surveys. The distributions of these galaxies by the absolute magnitude M_B are presented in two panels of Fig. 6. As one can see, the galaxies with distinct signs of unresolved nuclei have much greater luminosity with the average absolute magnitude $\langle M_B \rangle_{22} = -20.73 \pm 0.08$, while the other category of galaxies is characterized by the average absolute magnitude $\langle M_B \rangle_{00} = -18.73 \pm 0.13$. This difference agrees well with the data obtained by Davis et al. (2018), according to which the BH mass and the stellar mass of the galaxy are related with the steep relation

$$\log M_{BH} \sim (3.0 \pm 0.5) \times \log M_*$$

with a scatter of 0.68 dex. Let us note that this relation was derived by Graham et al. (2018) for 74 spiral galaxies in the Virgo cluster, where the properties of the BH candidates can be dependent on the density of galaxy environment. Sanchez-Janssen et al. (2018) recently noticed such an effect. That is why the relation between M_{BH} and M_* can be less scattered for solitary late-type galaxies.

However, it should be noticed that classical bulges show a correlation between black hole mass and bulge mass but pseudobulges do not (Kormendy & Ho, 2013). In fact, there is no correlation between pure-disk galaxies (e. g., disk mass) and black hole mass (see Figure 22 in the Kormendy & Ho (2013)).

We did not make it our purpose to investigate the photometric properties of unresolved nuclei in our sample. However, comparing face-on bulgeless galaxies and the objects studied by Graham et al. (2018), we conclude that typical masses of BH candidates among our galaxies are in the range of $\sim (10^3 - 10^5)M_\odot$.

According to Davis et al. (2017), BH masses show the closest correlation not with the stellar mass of a galaxy but with the spiral arm pitch angle ϕ :

$$\log M_{BH} \sim -(0.171 \pm 0.017) \times (|\phi^\circ| - 15^\circ).$$

Our sample of bulgeless galaxies, whose spiral pattern is not distorted by the projection effect, provides an opportunity to test the degree of correlation of M_{BH} with the pitch angle ϕ as well as with the presence of a bar in a galaxy.

Sometimes, central unresolved light sources are AGNs, not star clusters (e. g., NGC 4395, see Filippenko & Ho (2003) and Kormendy & Ho (2013)). Ho (2008) reviewed the subject of AGNs in galaxies such as those in our Table 1. Kormendy et al. (2010) provided black hole mass limits for several galaxies in Table 1. Interestingly, we found only a single galaxy, NGC 7798 = Mrk 332, among 220 face-on bulgeless galaxies that has a highly active nucleus. The nuclei of the rest bulgeless galaxies do not stand out with their strong emission. The existing steep relation between the nucleus luminosity and the total stellar mass of a galaxy allows one to avoid rough errors in estimating the galaxy distance. For example, the Sc galaxy NGC 4136

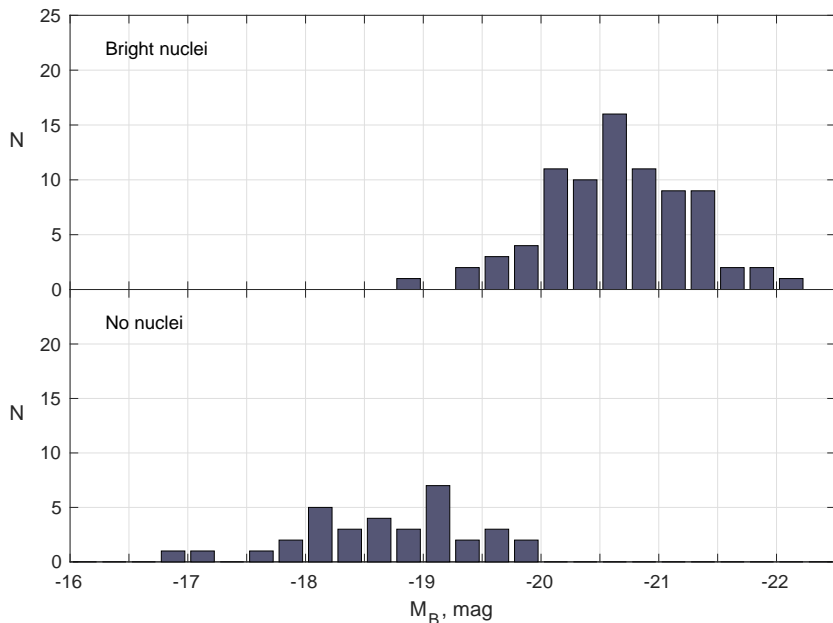


Figure 6. Distribution of face-on bulgeless galaxies with signs of the presence of unresolved nucleus (the top panel) and without any (the bottom panel) by absolute magnitudes.

with the radial velocity $V_{LG} = 560$ km/s and the apparent magnitude $B = 11.9^m$ has a distinct unresolved nucleus. With a Hubble distance of 8 Mpc, its absolute magnitude, -17.7^m , would not correspond to the presence of a noticeable nucleus (see Fig. 6). However, NGC 4136 is located in the “Local Velocity Anomaly” region known as Coma I (Kashibadze et al. 2018). Being actually at the Virgo cluster distance, 17 Mpc, this galaxy with $M_B = -19.3^m$ does not seem an exception to the general pattern. Thus, NGC 4136 is a possible new member of the peculiar association Coma I numbering about 30 members.

6 CONCLUDING REMARKS

Based on the data from Pan-STARRS1, SDSS, 2MASS, and HyperLEDA, we compiled a sample of face-on bulgeless galaxies. The sample includes 220 Sc–Scd–Sd galaxies distributed over the whole sky with the declinations $DEC > -30^\circ$. The galaxies have the angular diameters $d_{25} > 0.8'$, the typical inclination angle to the line of sight $i \sim 23^\circ$, and the median radial velocity ~ 5000 km/s. By its morphological composition and depth, the face-on bulgeless sample is close to the RFGC catalogue of flat galaxies; however, it contains a relatively smaller number of the Sd-type spirals than the sample of UF galaxies (Karachentseva et al. 2016).

About a half of the face-on bulgeless galaxies (43%) show the signs of bar-like structures, moreover, the bars can be found in the whole range of the absolute magnitudes M_B from -22^m to -17^m . Statistics of the spins of Sc–Scd–Sd face-on galaxies does not show any significant difference in the spin orientation of the spiral arms. A considerable amount of galaxies from our sample have slightly distorted peripheral spiral structures despite their apparent isolation.

According to our data, the pseudobulges of the Sc–Scd–Sd galaxies amount on average 11% of the total luminosity (stellar mass) of galaxies. Moreover, the largest representatives of this sample: M 101, IC 342, NGC 6946 are more robustly known to lack classical bulges according to Kormendy et al. ,2010. This suggests their classification as “bulgeless discs”.

Due to the negligible projection effect and slight internal extinction, our sample objects are quite suitable for studying the properties of central nuclei as possible BH candidates of moderate ($10^{3-5} M_\odot$) masses. Distinct unresolved nuclei in the K_s band in 2MASS and in the g, r, i, z, y bands in Pan-STARRS1 are observed in 40–60% of galaxies from our list. The presence of unresolved nucleus closely correlates with the luminosity of a galaxy, indirectly favouring the known steep relation $M_{BH} \sim M_*^3$. The properties of BH candidates in face-on bulgeless galaxies are worth careful studying, especially with the database of Spitzer images.

In our next paper we suppose to use the sample of face-on bulgeless galaxies together with the ultra-flat edge-on galaxy sample to elaborate the internal extinction effect in late-type galaxies as well as to determine star-formation rates in them. We also intend to estimate the occurrence of bulgeless galaxies in different cosmic structures in order to search for companions suitable to determine orbital masses from their motion.

Acknowledgements

The authors thank John Kormendy, the referee, for thorough examination of our manuscript and for very useful comments

and suggestions to improve the text. We are also grateful to Dmitry I. Makarov and Olga G. Kashibadze for their special assistance in the work that we have undertaken and for discussions. The work was performed within the SAO RAS state assignment in the part "Conducting Fundamental Science Research". The paper makes use of the data from the Pan-STARRS1, and the Two Micron All Sky Survey (2MASS) as well as from the HyperLEDA database (<http://leda.univ-lyon1.fr>).

References

- Abazajian K.N., Adelman-McCarthy J.K., Agueros M.A., et al., 2009, *ApJS*, 182, 54 (SDSS)
- Chambers K.C., Magnier E.A., Metcalfe N., et al. 2016, [arXiv:1612.05560](https://arxiv.org/abs/1612.05560) (Pan-STARRS1)
- Davis B.L., Graham A.W., Cameron E., 2018, [arXiv:1810.04888](https://arxiv.org/abs/1810.04888)
- Davis B.L., Graham A.W., Seigar M.S., 2017, *MNRAS*, 471, 2187
- de Vaucouleurs, G., de Vaucouleurs, A., and Corwin, H. G. 1976, *Second Reference Catalogue of Bright Galaxies*, Austin: University of Texas Press (RC2)
- Filippenko, A. V., & Ho, L. C. 2003, *ApJ*, 588, L1
- Graham A.W., Soria R., Davis B.L., 2018, [arXiv:1811.03232](https://arxiv.org/abs/1811.03232)
- Heidmann J., Heidmann N., de Vaucouleurs G., 1972, *MemRAS*, 75,85
- Ho, L. C. 2008, *ARA&A*, 46, 475
- Jarrett, T.N., Chester, T., Cutri R. et al., 2000, *AJ*, 119, 2498 (2MASS)
- Karachentsev I.D., Kaisina E.I., Kashibadze O.G., 2017, *AJ*, 153, 6
- Karachentsev I.D., Karachentseva V.E., Kudrya Y.N., 2016, *AstBu*, 71, 129
- Karachentsev I.D., Karachentseva V.E., Kudrya Y.N., et al., 1999, *AstBu*, 47, 5 (RFGC)
- Karachentsev I.D., Karachentseva V.E., Parnovsky S.L., 1993, *Astron. Nachr.* 314, 97 (FGC)
- Karachentseva V.E., Kudrya Y.N., Karachentsev I.D., Makarov D.I., Melnyk O.V., 2016, *AstBu*, 71, 1 (UF)
- Kashibadze O.G., Karachentsev I.D., Karachentseva V.E., 2018, *AstBu*, 73, 124
- Kim K., Oh S., Jeong H. et al., 2016, *ApJS*, 225, 6
- Kormendy, J. 2013, in *Canary Islands Winter School of Astrophysics, Volume XXIII, Secular Evolution of Galaxies*, ed. J. Falc3n-Barroso & J. H. Knapen (Cambridge: Cambridge University Press), 1
- Kormendy, J., & Ho, L. C. 2013, *ARA&A*, 51, 511
- Kormendy J., Drory N., Bender R., Cornell M., 2010, *ApJ*, 723, 54
- Kormendy, J. & Kennicutt, R.C., 2004, *ARA&A*, 42, 603
- Kormendy, J. 1993, in *IAU Symposium 153, Galactic Bulges*, ed. H. Dejonghe & H. J. Habing (Dordrecht: Kluwer), 209
- Kormendy, J. 1982, in *Twelfth Advanced Course of the Swiss Society of Astronomy and Astrophysics, Morphology and Dynamics of Galaxies*, ed. L. Martinet & M. Mayor (Sauverny: Geneva Observatory), 113
- Kormendy J., 1979, *ApJ*, 227, 714
- Lackner C.N., Gunn J.E., 2012, *MNRAS*, 421,2277
- Lange R., Moffett A.J., Driver S.P., et al. 2016, *MNRAS*, 462, 1470
- Makarov D., Prugniel P., Terekhova N., et al. 2014, *A & A*, 570A, 13 (HyperLEDA)
- Melnyk O.V., Karachentseva V.E., Karachentsev I.D., 2017, *AstBu*, 72, 1
- Oohama N., Okamura S., Fukugita M., et al. 2009, *ApJ*, 705, 245
- Parnovsky S.L., Karachentsev I.D., Karachentseva V.E., 1994, *MNRAS*, 268, 665
- Sanchez-Janssen R., Cote P., Ferrarese L., et al., 2018, [arXiv:1812.01019](https://arxiv.org/abs/1812.01019)
- Schlegel D.J., Finkbeiner D.P., & Davis M., 1998, *ApJ*, 500, 525
- Simard L., Mendel J.T., Patton D.R., et al. 2011, *ApJS*, 196, 11
- Simien F., de Vaucouleurs G., 1986, *ApJ*, 302, 517